Transmission Spectral Characteristics of Photonic Crystals Milled in Annealed Proton-Exchange $LiNbO_3$ Waveguide *

Quan-Zhou Zhao(赵全周)[1,2], De-Long Zhang(张德龙)[1**]

[1]*School of Precision Instruments and Optoelectronics Engineering, and Key Laboratory of Optoelectronic Information Science and Technology (Ministry of Education), Tianjin University, Tianjin 300072*

[2]*School of Physics and Electronic Engineering, Shanxi Datong University, Datong 037009*

(Received 28 October 2016)

Transmission spectra of triangular lattice photonic crystals milled in the top surface of an annealed proton-exchange waveguide are numerically simulated. The effects of the finite depth, conical shape, trapezoidal shape and hybrid shape of holes are theoretically analyzed. Due to the difficulty of milling high aspect-ratio cylindrical holes in lithium niobate ($LiNbO_3$), a compromised solution is proposed to improve the overlap between shallow holes and the waveguide mode, and useful transmission spectra with strong contrast and sharp band edges are achieved.

PACS: 42.70.Qs, 42.25.Dd, 42.25.Lc DOI: 10.1088/0256-307X/34/3/034207

Photonic crystals (PCs) have the potential applications to reduce the size and to increase the functionality of integrated optics devices.[1] To date, remarkable progress in the realization of high-quality PCs has been achieved mainly for silicon[2,3] and some other semiconductor materials. These materials possess high refractive indices, good optical transmission in the telecom wavelength range, and their microstructuring and nano-structuring are strongly supported by the advanced semiconductor technology. On the other hand, there is a strong interest in the development of high-density integrated photonic devices based on nonlinear optical materials, which offer the possibility of electro-optical modulation and switching. Lithium niobate ($LiNbO_3$) is an attractive substrate of photonic crystal structures for its excellent nonlinear electro-optical properties. However, producing good nanometric optical structures in $LiNbO_3$ is a difficult task due to its well-known resistance towards standard machining techniques like wet etching or reactive ion etching. Focused ion beam (FIB) etching seems to be the most attractive technique to perform nanometric-sized holes in $LiNbO_3$. Yin was the pioneer to obtain one-dimensional $LiNbO_3$ structure with features of 350 nm width and 1600 nm depth,[4] and Lacour *et al.*[5] have achieved a triangular lattice of submicrometric holes with depth of 2 μm. In Refs. [6,7], the authors calculated the transmission spectra with the two-dimensional finite-difference time-domain method and investigated the feasibility of tunable $LiNbO_3$ photonic crystals.[6] At the same time the superprism effects[8] have also been studied and demonstrated[9–11] in $LiNbO_3$, which have motivated a number of new micro-optical components such as superlenses,[12,13] negative refraction devices[12,14] and wavelength multiplexing/demultiplexing devices.[15,16]

Unfortunately, during fabrication some of the material removed by the focused ion beam tends to redeposit on the sample, the holes milled by focused ion beam are always characterized by finite depth and conical shape. Milling submicron-diameter holes with high aspect ratio is still challenging. In this work, we perform a theoretical study on the stop-band characteristics of PCs in an annealed proton-exchange (APE) $LiNbO_3$ waveguide, using the three-dimensional finite-difference time-domain method.[17] The study mainly focuses on the effects of the finite depth and non-cylindrical shape of holes on the stop-band characteristics of the PCs.

Figure 1(a) shows the schematic diagram of triangular lattice photonic crystals milled into an x-cut APE $LiNbO_3$ waveguide. Figure 1(b) shows the cross section of the waveguide. The lattice constant a is 480 nm and the hole radius is $r = 0.35a$. A coordinate system is fixed at the waveguide surface with the x-axis parallel to the depth direction of the substrate, the y-axis to the waveguide axis, and the z-axis to the width direction. The extraordinary index profile follows a Gaussian function in the depth x-direction for APE waveguide. The transmission spectra along the y-axis direction are calculated by the three-dimensional finite-difference time-domain method. Simulations are made within the domain

*Supported by the National Natural Science Foundation of China under Grant Nos 50872089, 61077039 and 61377060, the Research Grants Council of the Hong Kong Special Administrative Region of China under Grant No 11211014, the Key Program for Research on Fundamental to Application and Leading Technology of Tianjin Science and Technology Commission of China under Grant No 11JCZDJC15500, and the Specialized Research Fund for the Doctoral Program of Higher Education of China under Grant No 20100032110052.

**Corresponding author. Email: dlzhang@tju.edu.cn

© 2017 Chinese Physical Society and IOP Publishing Ltd

which contains a single row of holes along the light propagation direction y-axis, extends from 10 μm below to 2 μm above the top surface of the waveguide along the x-direction and is one lattice period in width along the z-direction. The x boundaries and the y boundaries are terminated with convolution PML[18] to absorb the outgoing radiation. Through periodic boundary conditions applied to the z boundaries an infinitely wide photonic crystal fabricated on a planar APE waveguide is represented. A Gaussian source $\exp(-x^2/(2d_x^2) - z^2/(2d_z^2))$ with $d_x = 1.5\,\mu\text{m}$ and $d_z = 20\,\mu\text{m}$ with maximum field located at 2.5 μm below the substrate surface is introduced at just one y boundary (4 μm upstream from the first hole). Transmission spectra are measured at the other y boundary (6 μm downstream after the last hole). An orthogonal Cartesian mesh is used, the grid-size $a/14$ along the x-axis, $a/16$ along the y- and z-axis are chosen, respectively. The curved hole-edges are modeled by the conformal dielectric technique.[19]

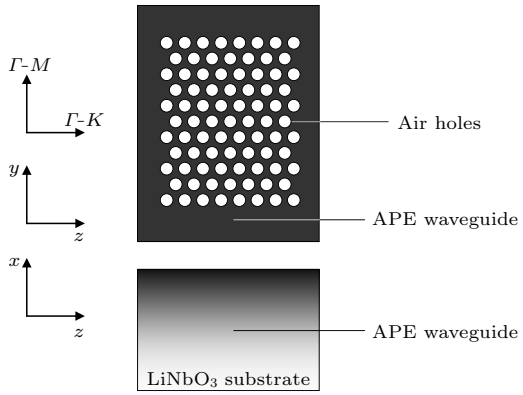

Fig. 1. (a) Schematic diagram of triangular lattice photonic crystals fabricated in an x-cut APE LN waveguide. (b) Cross section of an x-cut APE LN waveguide.

Simulated transmission spectra for $LiNbO_3$ photonic crystals containing 20 rows of cylindrical holes with depths 1, 2, 3, 4, 5 and 8 μm, respectively, are shown in Fig. 2(a). One can see that the effect of holes depth on the stop-band is evident. Holes with depths of 1 μm and 2 μm which do not reach the center of the optical mode ($x = 2.5\,\mu\text{m}$) result in nearly flat transmission spectra without strong spectral features. As the holes become deeper to overlap most of the waveguide mode, the contrast between the pass-band and stop-band and the sharpness of the band-edge become stronger and sharper. The continuous-wave light propagation inside the photonic crystals can be simulated to validate the above results. For the case of sufficiently deep cylindrical holes we have chosen two wavelengths that one is 1.3 μm inside the stop band and the other is 1.8 μm outside the stop band. Figures 2(b) and 2(c) show the propagating process for wavelength 1.3 μm and 1.8 μm, respectively. For wavelength 1.3 μm light is uniformly retro-reflected from the cylindrical holes, resulting in low transmittance through the photonic crystal structure. For wavelength 1.8 μm, light passes through the photonic crystals and into the un-patterned waveguide. The case of shallow holes is shown in Fig. 2(d). For wavelength 1.3 μm only the portion of the mode overlapping the holes is retro-reflected. The lower part of the mode passes under the holes without effect and continues as a guided mode of the downstream un-patterned APE waveguide.

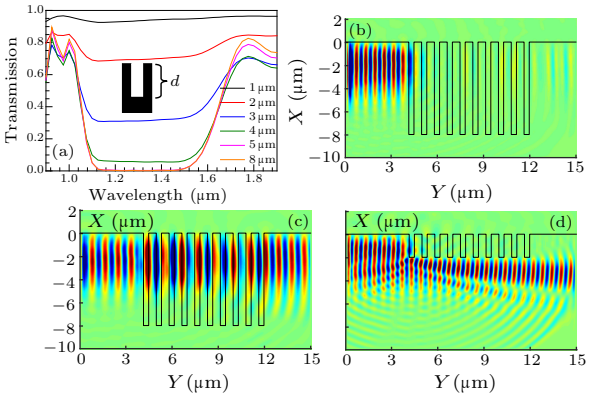

Fig. 2. (a) Transmission spectra of LN photonic crystals containing 20 rows of 1, 2, 3, 4, 5 and 8 μm deep cylindrical holes. (b) Continuous field (E_z) slices at $\lambda = 1.3\,\mu\text{m}$ for 8 μm deep cylindrical holes. (c) Continuous field (E_z) slices at $\lambda = 1.8\,\mu\text{m}$ for 8 μm deep cylindrical holes. (d) Continuous field (E_z) slices at $\lambda = 1.3\,\mu\text{m}$ for 2 μm deep cylindrical holes.

Figure 3(a) shows the simulated transmission spectra for $LiNbO_3$ photonic crystals containing 20 rows of conical holes with depths of 1, 2, 3, 4, 5 and 8 μm, respectively. For the conical holes the transmission spectra do not have spectral features that could be considered as a stop band. At the same time the conical holes produce great losses. As conical holes are etched deeper, the overall transmittance decreases uniformly. The transmittance almost approaches zero in the case of conical hole of 8 μm depth. Figure 3(e) shows the continuous-wave light propagation for 8 μm deep cones and a wavelength 1.7 μm light. The incident light is refracted towards the bottom of the substrate. Thus the loss is very great for conical holes. However, if the conical holes become deeper and deeper, the sidewall angles become closer and closer to 0°, and the stop-bands appear again. The results for conical holes with depths of 8, 10, 15, 20, 30 and 40 μm are shown in Fig. 3(b). For conical holes with depths of 8, 10 and 15 μm the transmission spectra are flat without spectral features. For conical holes with depths of 20, 30 and 40 μm the stop-band appears again. The sidewall angle is about 0.5° for 20 μm deep cone. The sidewall angles for 30 and 40 μm deep cone are less than 0.5°. Thus useful transmission spectra can be produced for the conical holes if the sidewall angle is within 0.5° with respect to the vertical.

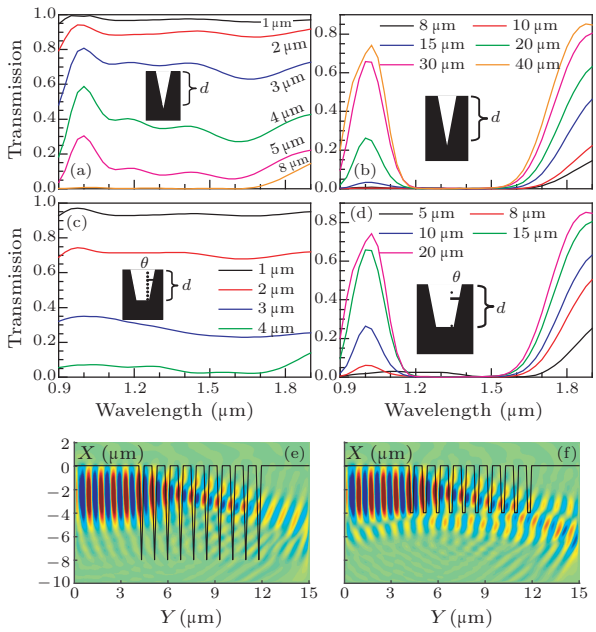

Fig. 3. (a) Transmission spectra of LN photonic crystals containing 20 rows of 1, 2, 3, 4, 5 and 8 μm deep conical holes. (b) Transmission spectra of LN photonic crystals containing 20 rows of 8, 10, 15, 20, 30 and 40 μm deep conical holes. (c) Transmission spectra of LN photonic crystals containing 20 rows of 1, 2, 3 and 4 μm deep trapezoidal holes. (d) Transmission spectra of LN photonic crystals containing 20 rows of 5, 8, 10, 15 and 20 μm deep trapezoidal holes. (e) Continuous field (E_z) slices at $\lambda = 1.7$ μm for 8 μm deep conical holes. (f) Continuous field (E_z) slices at $\lambda = 1.7$ μm for 4 μm deep trapezoidal holes.

The results of trapezoidal holes are similar to the results of conical holes. Figure 3(c) shows the simulated transmission spectra for $LiNbO_3$ photonic crystals containing 20 rows of 1, 2, 3 and 4 μm deep trapezoidal holes whose top radius and bottom radius are $0.35a$ and $0.175a$, respectively. The transmission spectra also have no spectral features. The deeper the holes are, the greater the loss is. Figure 3(f) shows the continuous-wave light propagation for 4 μm deep trapezoidal holes and a wavelength 1.7 μm light. The incident light is refracted towards the bottom of the substrate. When the trapezoidal holes become deeper and deeper, the stop-bands appear again. The results for trapezoidal holes with depths of 5, 8, 10, 15 and 20 μm are shown in Fig. 3(d). For the trapezoidal holes with depths of 5 and 8 μm the transmission spectra are flat without spectral features. For trapezoidal holes with depths of 10, 15 and 20 μm the stop-bands appear again. The sidewall angles for 10, 15 and 20 μm deep trapezoid are within 0.5°.

As described above, it is difficult to fabricate deep, high aspect-ratio holes with a near-perfect cylindrical profile over most of the depth in LN. One usually obtains the holes with a cylindrical-conical hybrid shape as shown in the inset of Fig. 4(a). Next we turn to discuss the stop band characteristic of the cylindrical-conical hybrid holes. We assume a constant hole depth of 4.5 μm where the top portion of height d is perfectly cylindrical and the bottom portion is conical over the remaining height $(4.5 - d)$ μm. The simulations are carried out by changing the cylindrical portion of the holes d from 1 to 4.5 μm in a step of 0.5 μm. Figure 4(a) shows the results. When the cylindrical portion is 3.5 μm or more in depth, the transmission spectra exhibit sharp band-edges and strong contrast. When the cylindrical portion decreases, the contrast begins to weaken. For those hybrid holes whose cylindrical depth is less than 2 μm the transmission spectra have been distorted seriously. The cylindrical portion determines the desired spectral features of the stop band.

Fabricating such deep high-aspect holes with a near-perfect cylindrical profile over most of the depth is difficult in $LiNbO_3$. To obtain a useful stop-band we propose a feasible, compromised solution to fabricate PCs in LN. The solution suggests that some portion of the top surface is first removed (by FIB) to form a low-aspect trench at the waveguide surface and then shallower holes are milled at the bottom of the trench. The shallower holes still overlap the most portion of optical mode. Making such a trench in the waveguide will cause loss obviously. Figure 4(b) shows the transmission spectra of waveguide etched with a wide trench having a constant length of 9 μm along the propagation direction and depths varying from 0.5 μm to 3 μm. The losses are about 7% and 16% for 1-μm-deep and 1.5-μm-deep trenches.

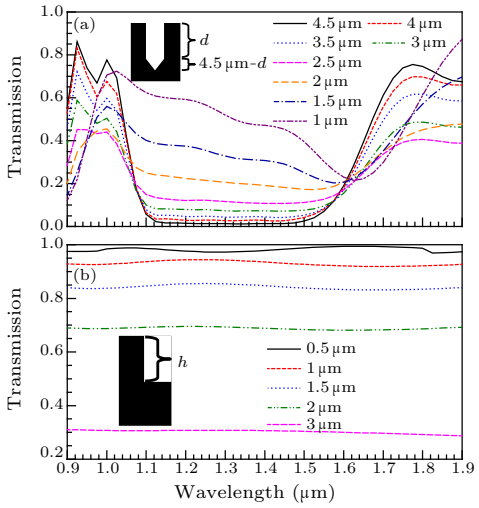

Fig. 4. (a) Transmission spectra of LN photonic crystals containing 20 rows of 4.5 μm deep hybrid holes where the top portion of height d is perfectly cylindrical and the bottom portion is conical over the remaining height 4.5 μm. (b) Transmission spectra of x-cut APE LN waveguide with a wide trench having a constant length of 9 μm along the propagation direction and depths ranging from 0.5μm to 3 μm.

Figure 5 shows the transmission spectra of LN photonic crystals with holes milled at the bottom of a shallow trench. Figures 5(a) and 5(b) show the results

for a trench of 1 μm depth, while Figs. 5(c) and 5(d) show the results for a trench of 1.5 μm depth. In all the cases, the trench is 9 μm in length along the y-axis. In Figs. 5(a) and 5(c) the holes are cylindrical and range from 1 μm to 4 μm in depth, and in Figs. 5(b) and 5(d) the holes are cylindrical over the top 75% of their depth, and are conical over the bottom 25%. Figure 5 clearly shows the importance of the cylindrical shape. Even if the conical portion has only the bottom 25% of their depth, it has a significant effect on the contrast between the pass-band and stop-band compared to Figs. 5(a) and 5(b) or Figs. 5(c) and 5(d). Figure 5(d) shows that photonic crystals with hybrid holes of 3 μm total depth (cylindrical over the top 2.25 μm) etched at the bottom of 1.5 μm deep trench can produce useful transmission spectra with strong contrast and sharp band edges.

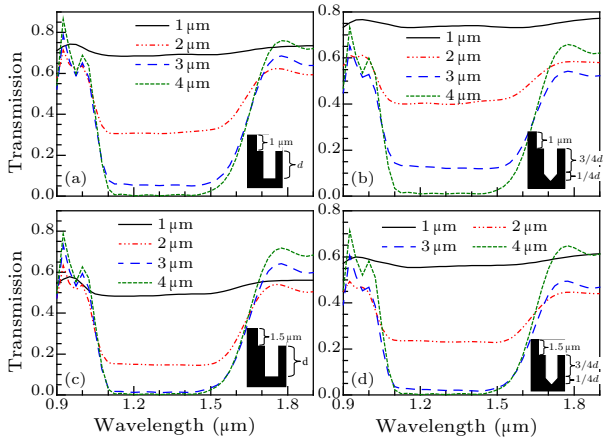

Fig. 5. Transmission spectra for photonic crystals etched at the bottom of a shallow trench. (a, b) A trench of 1 μm depth, and (c, d) a trench of 1.5 μm depth. For (a) and (c), cylindrical holes' depths range from 1 μm to 4 μm, and for (c) and (d) the hybrid holes' total depths range from 1 μm to 4 μm, where the top 75% of the hole is cylindrical and the bottom 25% is conical.

In conclusion, we have analyzed the transmission spectra of triangular lattice photonic crystals milled in the top surface of an APE $LiNbO_3$ waveguide. The effects of cylindrical hole-depth, conical shape, trapezoidal shape and hybrid shape of holes on the transmission spectra are analyzed. Cylindrical holes which are sufficiently deep to overlap most of the waveguide mode produce useful transmission spectra with strong contrast and sharp band edges. For conical and trapezoidal holes the transmission spectra without spectral features are produced unless the sidewall angle is within 0.5° from the vertical. The cylindrical portion of the hybrid hole determines the desired spectral features of the stop-band. Because fabricating high-aspect holes with a near-perfect cylindrical profile over most of the depth is difficult in $LiNbO_3$, we propose to remove some portion of the top waveguide surface first to form a shallow trench on the waveguide surface, and then mill the holes at the bottom of the trench. The simulation shows that shallow hybrid holes can produce transmission spectra with strong contrast and sharp band edges.

References

[1] Joannopoulos J D et al 2008 *Photonic Cryst.: Molding Flow Light* 2nd edn (Princeton: Princeton University Press)
[2] Akahane Y et al 2003 *Nature* **425** 944
[3] Almeida V R et al 2004 *Nature* **431** 1081
[4] Yin S 1999 *Microwave Opt. Technol. Lett.* **22** 396
[5] Lacour F et al 2005 *Opt. Mater.* **27** 1421
[6] Roussey M et al 2005 *Appl. Phys. Lett.* **87** 241101
[7] Roussey M et al 2007 *J. Opt. Soc. Am.* B **24** 1416
[8] Kosaka H et al 1998 *Phys. Rev.* B **58** R10096
[9] Amet J et al 2008 *Photon. Nanostruct. Fundam. Appl.* **6** 47
[10] Diziain S et al 2008 *Appl. Phys. Lett.* **93** 261103
[11] Bernal M P et al 2011 *Appl. Phys. Lett.* **98** 071101
[12] Gralak B et al 2000 *J. Opt. Soc. Am.* A **17** 1012
[13] Hu X et al 2004 *Appl. Phys. Lett.* **85** 1520
[14] Shelby R A et al 2001 *Science* **292** 77
[15] Lupu A et al 2004 *Opt. Express* **12** 5690
[16] Matsumoto T et al 2005 *Opt. Express* **13** 10768
[17] Taflove A and Hagness S C 2005 *Comput. ElectroDyn.: Finite-Difference Time-Domain Method* 3rd edn (Boston: Artech House)
[18] Roden J A et al 2000 *Microwave Opt. Technol. Lett.* **27** 334
[19] Yu W et al 2001 *IEEE Microwave Wireless Compon. Lett.* **11** 25